applied sciences

MDPI

Article

Estimation Equation for Horizontal Load Bearing Capacity of Circular PCFST with Diaphragm

Seiya Zenzai [1], Yuki Chikahiro [2,*] and Shigeru Shimizu [2]

[1] C.E. Management Integrated Laboratory Co., Ltd., Amenomiya 2347-3, Nagano 387-0001, Japan
[2] Department of Water Environment and Civil Engineering, Shinshu University, Wakasato 4-Chome, Nagano 380-8553, Japan
* Correspondence: chikahiro@shinshu-u.ac.jp

Abstract: The purpose of this study is to propose a practical formula for estimating the maximum load bearing capacity of partially concrete-filled steel tubes (PCFST) without using complicated numerical analysis and estimation procedures. This study focused on four parameters (radius thickness ratio R, slenderness ratio λ, axial force ratio n, and concrete filling ratio L_c/L) used in numerical analysis to determine horizontal load bearing capacity and buckling position in PCFST with diaphragms under monotonic loading. Based on the results, an equation for estimating the horizontal load bearing capacity of PCFST was obtained by nonlinear regression analysis. The estimation equation that did not consider different buckling positions predicted the horizontal load bearing capacity with an error of approximately ±10% from the numerically analyzed values, but the estimation equation that took the different buckling positions into consideration could predict the horizontal bearing capacity to within a margin of error of about 5% from the numerical value by determining the buckling position in advance.

Keywords: partially concrete-filled tubes; circular section tubes; estimation equation; horizontal load bearing capacity

Citation: Zenzai, S.; Chikahiro, Y.; Shimizu, S. Estimation Equation for Horizontal Load Bearing Capacity of Circular PCFST with Diaphragm. *Appl. Sci.* **2022**, *12*, 8739. https://doi.org/10.3390/app12178739

Academic Editor: Laurent Daudeville

Received: 10 August 2022
Accepted: 29 August 2022
Published: 31 August 2022

1. Introduction

A partially concrete-filled steel tube (PCFST) structure is a steel tube of circular or rectangular cross-section that is partially filled with concrete at the bottom part. The infilled concrete prevents the steel plate from buckling into the steel tube, and the restraint of the steel tube increases the compressive strength of the concrete, resulting in a significant improvement in strength, toughness, and stiffness compared to hollow steel tubes with no concrete.

In Japan, the PCFST structure was focused on after the Kobe Earthquake occurred in 1995, which caused severe infrastructure damage. The results of a survey of the damage from that earthquake [1] showed that PCFST structures have excellent seismic performance, and research on PCFST structures, whether circular or rectangular in cross-section, are actively conducted. For example, for PCFST structures with circular cross-sections, experiments have been conducted to define the limit state [2,3], to clarify their behavior with the diagram under static and dynamic loadings [4,5], and to develop accurate numerical models [6,7]. In addition, Iura et al. proposed an estimation method for the horizontal load bearing capacity of concrete-filled circular section piers [8]. They proposed an equation for estimating the maximum horizontal load bearing capacity of concrete-filled circular piers under cyclic horizontal loading, using experimentally obtained maximum bending moment and plastic section coefficients. Although their equation agreed well with experimental data, it required numerical integration of the cross-sectional data, and the maximum load bearing capacity cannot be easily obtained using only parameters obtained during pier design.

Therefore, the purpose of this study is to propose a practical formula for estimating the maximum load bearing capacity of tubes without using complicated numerical analysis and estimation procedures. To clarify their effects on horizontal load bearing capacity and buckling position, the parametric analysis on concrete-filled circular section tubes with diaphragm under monotonic loading was conducted focusing on design parameters such as thickness ratio, slenderness ratio, axial force ratio, and concrete filling ratio. Furthermore, an equation for estimating the horizontal load bearing capacity of concrete-filled tubes was discussed by nonlinear regression analysis.

2. Numerical Finite Element Model

2.1. Outline

The numerical model is outlined in Figure 1. It uses a circular section without stiffeners in the vertical direction, with a diaphragm placed directly above the concrete inside the steel tube. The diaphragm has the effect of smoothly transferring compressive forces to the concrete and preventing the progression of buckling even after the maximum bearing capacity. L, L_c, D, and t in the figure indicate the height of the steel tube, the height of the concrete, and the diameter and thickness of the steel tube, respectively.

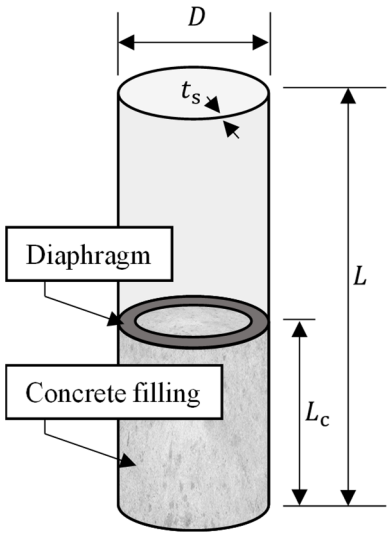

Figure 1. Numerical model.

The specifications of each numerical model are shown in Table 1. The radius thickness ratio parameter R and the slenderness ratio parameter λ in the table are expressed by the following equations by Specifications for highway bridges in Japan [9]:

$$R = \sqrt{3(1-\mu_s^2)}\frac{f_s}{E_s}\frac{D}{2t} \quad (1)$$

$$\lambda = \frac{KL}{r}\frac{1}{\pi}\sqrt{\frac{f_s}{E_s}} \quad (2)$$

where μ_s, f_s, E_s, K, and r are Poisson's ratio, yield stress, Young's modulus, the effective buckling length factor of the cantilevered beam, and the secondary radius of the section of steel tube, respectively. Based on the parameter limits defined in the Japanese Specifications for Highway Bridges [9], R $(0.03 \leq R \leq 0.12)$ is set to 0.06, 0.09, and 0.12, and λ $(0.2 \leq \lambda \leq 0.4)$ is set to 0.2, 0.3, and 0.4. The axial compressive force acting on the column head ranged from 10% to 50% of the yield axial force of the steel tube only, excluding the in-filled concrete.

Table 1. Numerical model specifications.

Model	C-006-020	C-006-030	C-006-040	C-009-020	C-009-030	C-009-040	C-012-020	C-012-030	C-012-040
Diameter of steel tube D [mm]	900								
Thickness of steel tube t_s [mm]	18			12			9.3		
Height of steel tube L [mm]	2550	3850	5100	2600	3850	5100	2600	3850	5100
Radius thickness ratio parameter R	0.06			0.09			0.12		
Slenderness ratio parameter λ	0.20	0.30	0.40	0.20	0.30	0.40	0.20	0.30	0.40
Axial force ratio n	0.1, 0.2, 0.3, 0.4, 0.5								
Concrete filling ratio L_c/L	0.2, 0.4, 0.6								

The stress-strain curve of the steel is shown in Figure 2. Young's modulus E_s, Poisson's ratio μ_s, and yield stress f_s were set to 206 GPa, 0.3, and 308 MPa, respectively, based on material tests obtained from a report on cyclic load testing of concrete-filled circular section bridge piers conducted at the Public Works Research Institute [10]. The von Mises yield condition was adopted as the yield criterion. For the concrete, the uniaxial compressive strength f_c was set to 22.0 MPa, Young's modulus $E_c = 4730\sqrt{f_c} = 21.0$ GPa, and Poisson's ratio μ_c was set to 0.2 according to ACI Committee 318 [11]. For the concrete, the stress-strain curve (Figure 3) was referred to the Popovics model and made into a multilinear form [12]. For the yield condition, the Drucker–Prager failure criterion was used as expressed in the following equation:

$$f_c = \alpha I_1 + \sqrt{J_2} \quad (3)$$

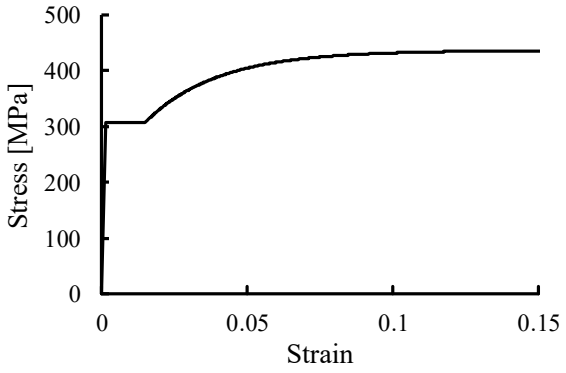

Figure 2. Steel tube stress-strain curve.

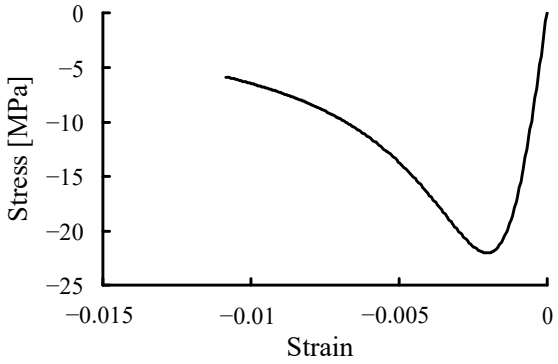

Figure 3. Compressive stress–compressive strain curve for concrete filling.

Here, I_1 is the first invariant of the stress tensor, J_2 is the second invariant of the deviatoric stress tensor, and the material constant α is assumed to be 0.2 based on Balmer's triaxial compression test [13]. Cracking due to tensile stress in concrete was taken into account by assuming cracking locations as described below.

2.2. Finite Element Model

Figure 4 shows the numerical model with a mesh partition. MSC's commercial FEM software (Marc2016) was used for the numerical analysis. Four-node shell elements were used for the steel tube and diaphragm, and eight-node brick elements were applied to model the concrete. A two-node beam element was employed to the top of the column in order to reduce the number of degrees of freedom and act axial load on centroid of tube. As mentioned above, we adopt linear elements in our discretization of the FE model. This is to reduce the effect of element aspect ratio degradation under the large deformation and to stabilize the contact normal between steel tube and concrete. A gap of 0.1 mm was provided between the steel tube and diaphragm elements and the concrete elements to allow for drying shrinkage of the concrete inside the steel tube.

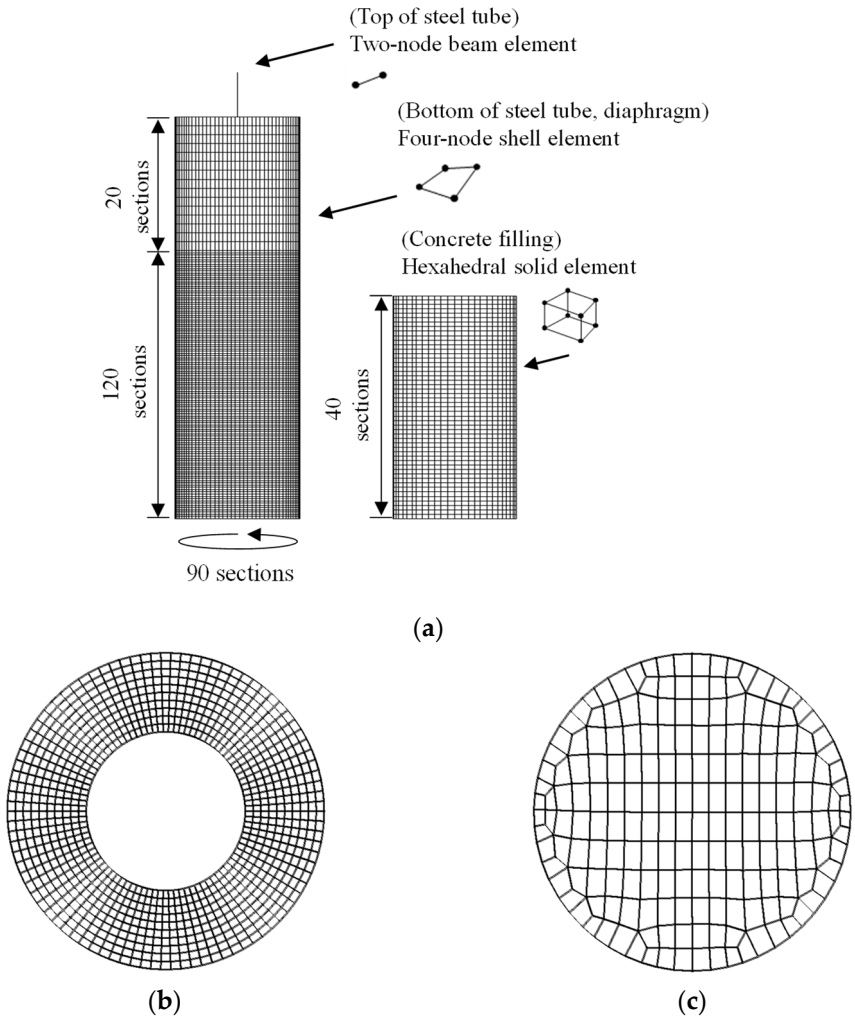

Figure 4. Sectioning of elements in the numerical model: (**a**) Steel tube and concrete; (**b**) Diaphragm; (**c**) Concrete section.

2.3. Numerical Conditions

Figure 5 shows the boundary conditions of the numerical model. The base has a fixed support, and the top of the column is subjected to axial compressive force N and horizontal displacement δ. When the concrete-filled steel tube is subjected to a load, contact,

separation, and friction occur between the steel members and the concrete. In this study, these behaviors are considered to be contact problems. The Coulomb friction law is used to model the behavior between the steel members and the concrete (Figure 6). The coefficient of friction between them, μ_{SC} was set to 0.2 based on Johansson's research [14].

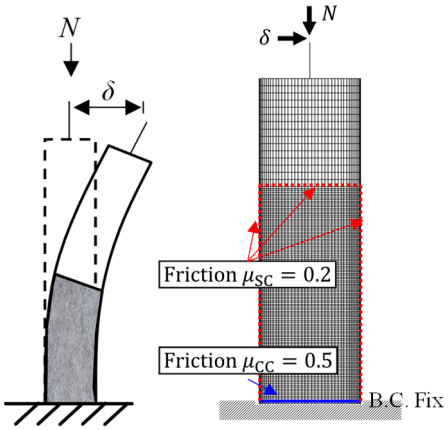

Figure 5. Numerical model boundary conditions.

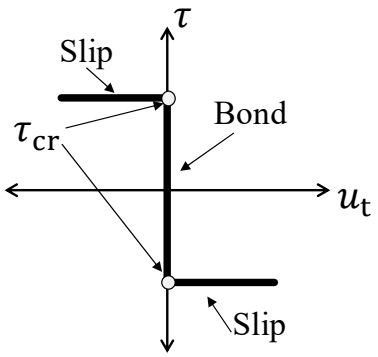

Figure 6. Coulomb's friction law.

As to the concrete's cracking behavior, Ngo et al. analyzed reinforced concrete beams, assuming the location of cracks and inserting a nonlinear spring into the assumed crack surface [15]. The advantage of this method is that a convergent solution can be obtained even when the deformation of the concrete becomes large. In this study, the location where the cracks in the concrete occur is assumed to be the bottom of the column because the bending moment is the largest at the bottom of the column under the horizontal load, and this crack is treated as the contact problem between the concrete interface and the rigid body inserted at bottom. This crack, that is the distance between the concrete interface and rigid body, becomes large when the bending moment acting on the column becomes large. The friction coefficient μ_{CC} between the two is set to 0.5. Note that the validity of these modeling methodologies in PCFST with circular cross-sections between the numerical model and the experiments has been confirmed in our previous study [5].

3. Behavior of Partially Concrete-Filled Steel Tubular (PCFST) Columns

In this section, model C-009-030 is used as a representative example to show the failure modes and load-displacement curves of the PCFST to understand the behavior of PCFST under horizontal loads.

3.1. Load-Displacement Curve and Equivalent Stress Distribution

For the range of models used in this study, three types of failure modes were observed in the PCFST as shown in Figure 7. Each model in the figure has the same radius thickness ratio and slenderness ratio, with only the axial force ratio being varied. In Figure 7a,

out-of-plane deformation occurred in the steel tube at the base of the column, while in Figure 7b, out-of-plane deformation occurred at two locations: in the steel tube at the base of the column and just above the concrete. In Figure 7c, out-of-plane deformation occurred in the steel tube directly above the concrete.

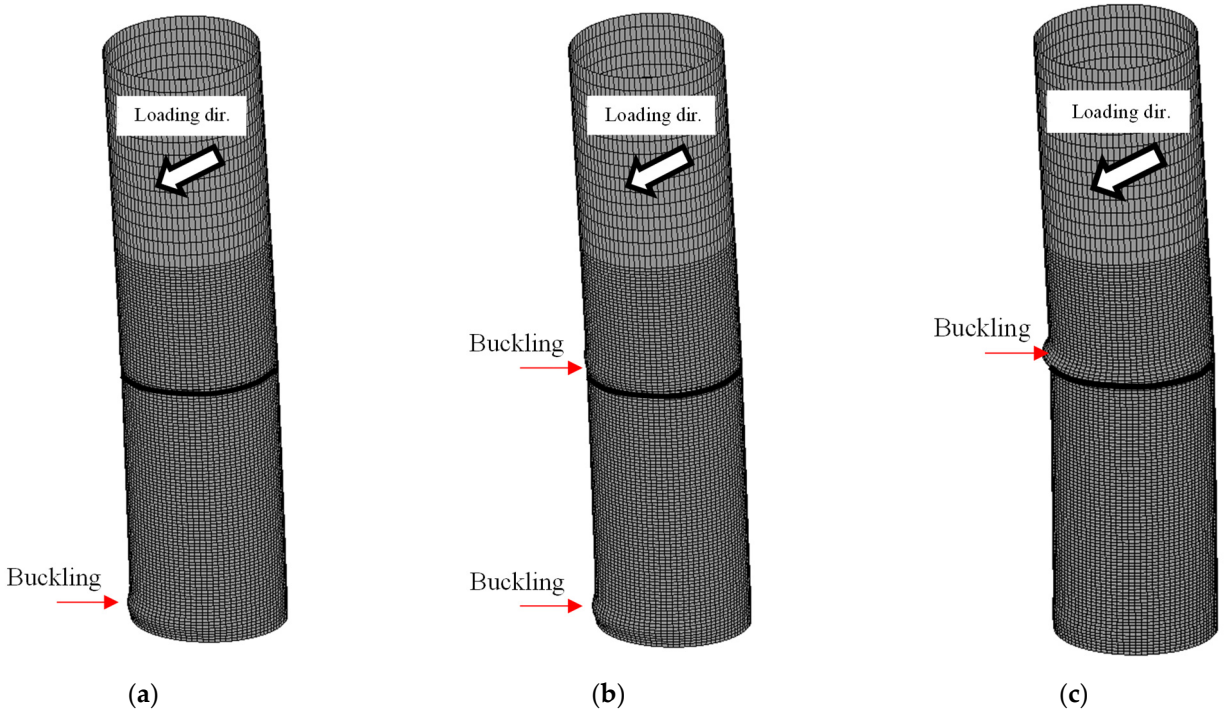

Figure 7. Typical failure modes (C-009-030, $L_c/L = 0.4$): (**a**) $n = 0.1$; (**b**) $n = 0.2$; (**c**) $n = 0.3$.

Figure 8 shows the load-displacement curves of the PCFST for each axial force ratio. The slope of the curves decreased as displacement increased for all the models. However, no obvious strength degradation can be seen, and load bearing capacity remained almost constant for models with failure modes shown in (a) and (b). On the other hand, for model (c), where the steel tube just above the concrete deformed out of plane, the horizontal load fell sharply after a horizontal displacement of 60 mm, similar to hollow steel tubes. These results show that there are different load bearing mechanisms for the model with out-of-plane deformation in the steel tube just above the concrete and other models with different failure modes.

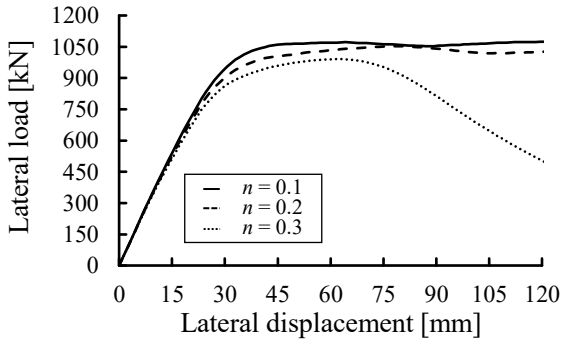

Figure 8. Lateral load versus lateral displacement (C-009-030, $L_c/L = 0.4$).

Figure 9 shows the equivalent stress distribution of the PCFST at the horizontal displacement of 60 mm. The right side of the figure shows the steel tube, and the left side shows the concrete filling. At this stage, the steel tube had high equivalent stress at the base or just above the diaphragm. The concrete filling had high equivalent stress at the interface with the diaphragm and at the base on the compression side. In addition, high equivalent

stresses were observed on the top surface of the concrete filling around the periphery of the diaphragm. This is a similar trend to that observed in the authors' study of PCFST's diaphragms [5].

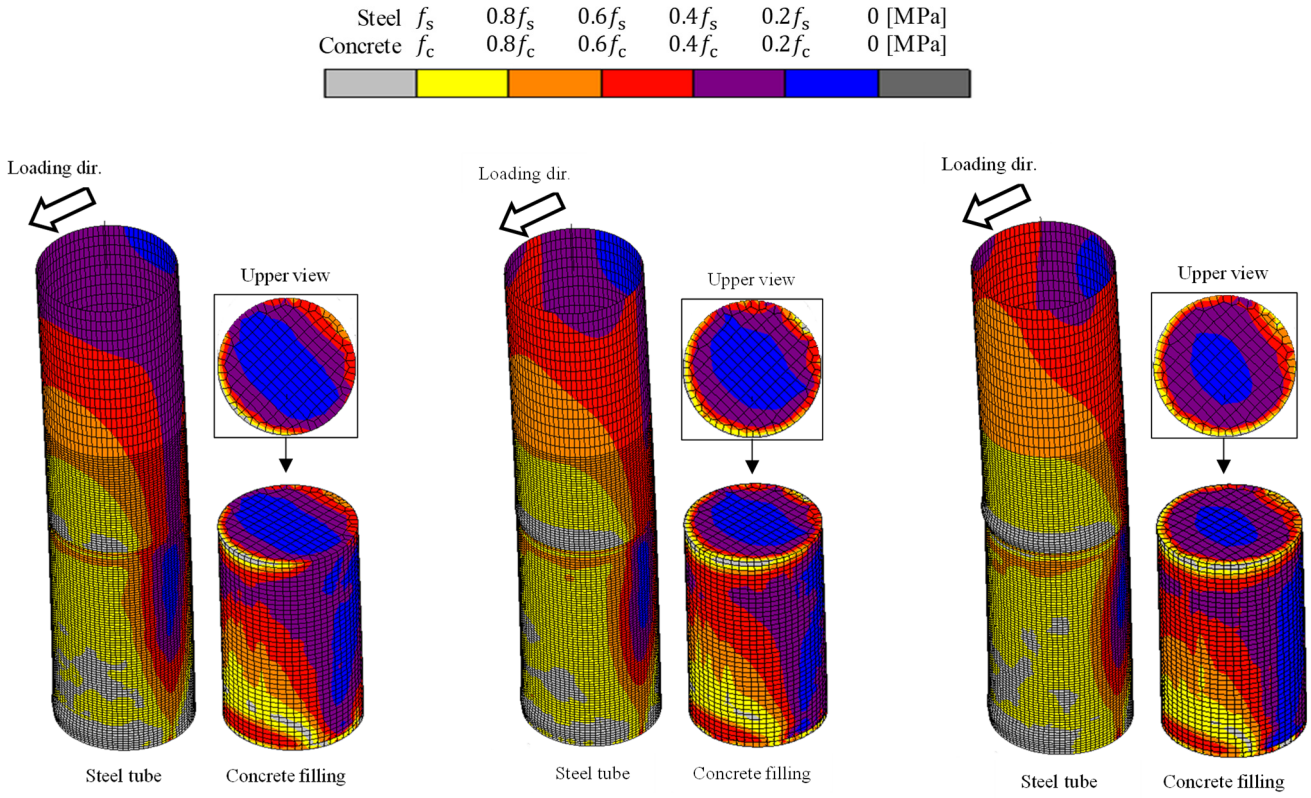

Figure 9. Equivalent stress distribution for steel tube and concrete filling at horizontal displacement of 60 mm (C-009-030, $L_c/L = 0.4$): (**a**) $n = 0.1$; (**b**) $n = 0.2$; (**c**) $n = 0.3$.

Figure 10 shows the normalized axial load on the steel tubes and concrete. Here, the normalized axial load is obtained by dividing each axial load by the acting axial force N. The axial load of the steel tube and concrete in the figure was calculated from the sum of the axial reaction forces on the base elements. Similar to the load-displacement curve, the hysteresis of the model where out-of-plane deformation occurred in the steel tube at the base of the column and the model where out-of-plane deformation occurred in two locations, in the steel tube at the base of the column and just above the concrete, are very similar, with the axial compressive force in the steel tube decreasing and turning into axial tensile force as displacement increased. In contrast, the axial compressive force acting on the concrete increased as shown in (a) and (b) of Figure 10. Meanwhile, for model (c) in Figure 10, where the steel tube directly above the concrete is deformed out of plane, the axial compressive force acting on the concrete grew larger while the axial force in the steel tube decreased, which is similar to other failure modes at the start of loading. However, the axial force in the concrete decreased and the steel tube shouldered a larger portion of the axial compressive force after a displacement of 60 mm. This is because the concrete did not bear the force after out-of-plane deformation occurred just above the concrete, as shown in Figure 10c.

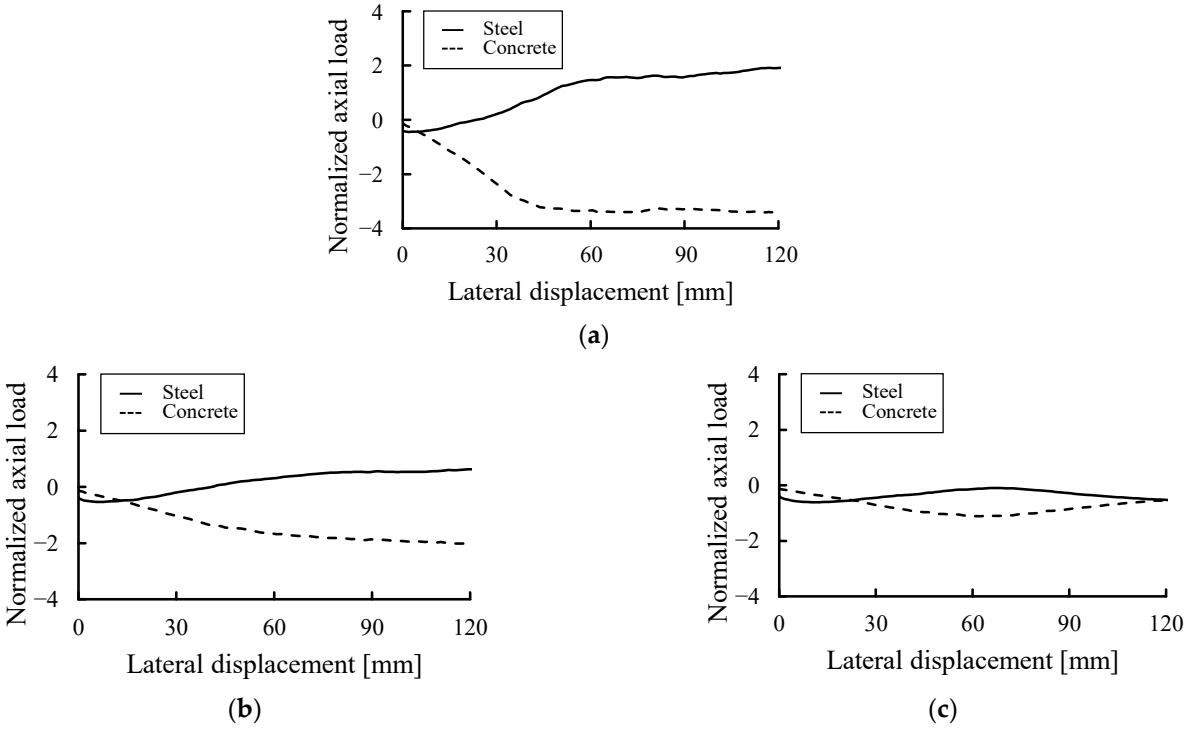

Figure 10. Normalized axial load versus lateral displacement (C-009-030, $L_c/L = 0.4$): (**a**) $n = 0.1$; (**b**) $n = 0.2$; (**c**) $n = 0.3$.

The results above indicate that load bearing capacity can be maintained even after out-of-plane deformation of the steel tube occurs due to increasing horizontal load. This is because the concrete bears the axial compressive force in the model where out-of-plane deformation occurs in the steel tube at the base of the column and the model where out-of-plane deformation of the steel tube occurs in the two locations discussed above. On the other hand, for the model where the steel tube directly above the concrete deformed out of plane, only the steel tube bore the axial force, which was not transmitted to the concrete because out-of-plane deformation occurred on the unfilled part of the steel tube. This may have caused the sudden degradation in strength.

3.2. Buckling Pattern

Table 2 shows the failure modes of all models, as demonstrated by model C-009-030 discussed in the previous section. Table 2a–c show the results for models with radius thickness ratios $R = 0.06$, 0.09, and 0.12, respectively. In the table, black sections show cases where out-of-plane deformation occurred in the steel tube at the base of the column, gray sections show cases where out-of-plane deformation occurred in both locations, and white sections show cases where out-of-plane deformation occurred in the steel tube just above the concrete.

The table shows that both the concrete filling ratio and axial force ratio affect the failure mode of the column when the models have the same radius thickness ratio parameter R and slenderness ratio parameter λ. Increasing the concrete filling ratio tended to cause buckling at the base of the steel tube, while higher axial force ratios tended to increase buckling of the steel tube directly above the concrete. Moreover, with the same radius thickness ratio parameter R and different slenderness ratio parameter λ, the buckling positions for concrete filling ratios L_c/L and axial force ratios n are almost the same, with no apparent effect from the slenderness ratio parameter λ. On the other hand, with the same slenderness ratio parameter λ and different radius thickness ratio parameters R, buckling occurred in the steel tube directly above the concrete under smaller axial forces for models with larger radius thickness ratio parameters.

Table 2. Relationship between buckling position and design parameters: (**a**) Model with $R = 0.06$; (**b**) Model with $R = 0.09$; (**c**) Model with $R = 0.12$.

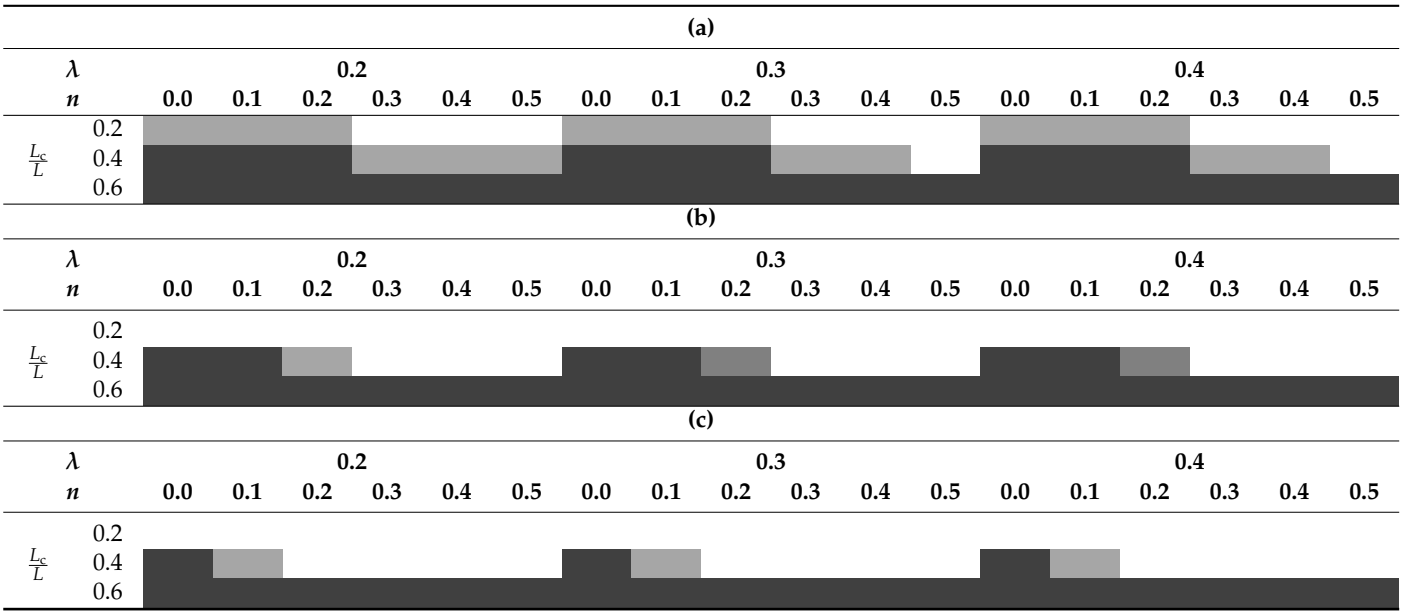

4. Estimation Equation for Maximum Load Bearing Capacity

4.1. Proposed Estimation Equation

Based on the results of the numerical analysis, an equation for estimating the maximum load bearing capacity was obtained by nonlinear regression analysis using the statistical analysis software R. The equation for estimating the maximum load bearing capacity is as follows:

$$\frac{P}{P_u} = \left(7.1 \times \frac{L_c}{L}^{0.68} \times R^{1.04} \times \lambda^{-0.07}\right) - \left(4.45 \times \frac{L_c}{L}^{-0.65} \times R^{0.72} \times \lambda^{0.3} \times n^{1.43}\right) + 1.01 \quad (4)$$

Here, P_u is the maximum bearing capacity at $L_c/L = 0$ and $n = 0$ for each model. In other words, the maximum load bearing capacity of the PCFST can be estimated according to the concrete filling height L_c/L, axial force ratio n, radius thickness ratio R and slenderness ratio λ, as long as P_u can be obtained for a steel tube without complicated contact problems.

4.2. Applicability of Estimation Equation

4.2.1. Results for Varying Slenderness Ratios

Figure 11 shows the maximum load bearing capacities for the numerical and estimated values for models with slenderness ratios λ of 0.2 and 0.4, respectively. The vertical axis shows the non-dimensionalized horizontal load bearing capacity P/P_u, and the horizontal axis shows the axial force ratio n. Open and closed dots in the figure show the results of the numerical analysis. Open dots indicate buckling just above the concrete, and closed dots indicate buckling at the base of the steel tube and in both locations, at the base of the steel tube and just above the concrete. The estimated values are indicated by dashed lines in the figure.

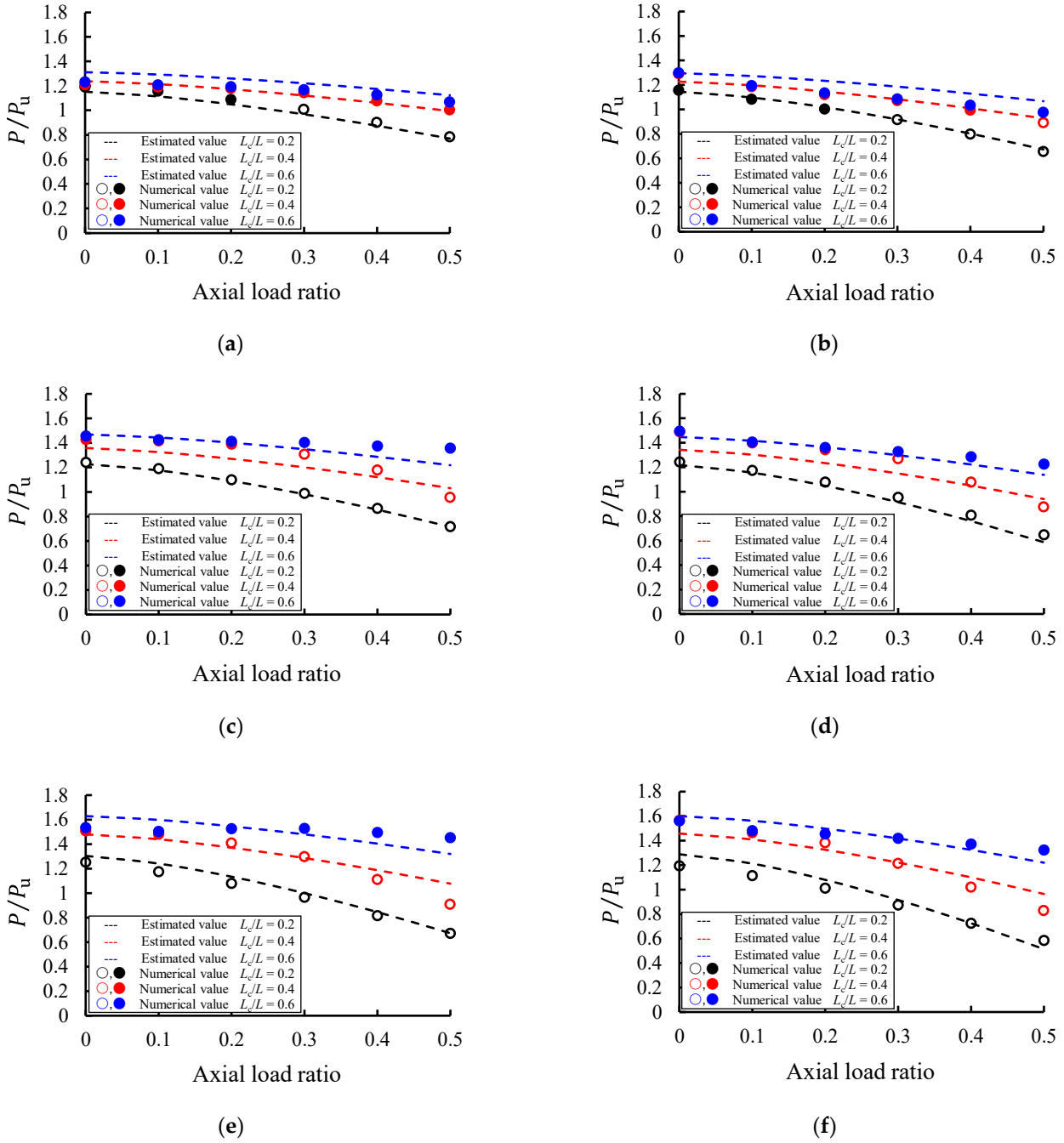

Figure 11. Maximum load bearing capacity and estimation equation for each model: (**a**) Model C-006-020; (**b**) Model C-006-040; (**c**) Model C-009-020; (**d**) Model C-009-040; (**e**) Model C-012-020; (**f**) Model C-012-040.

Firstly, focusing on Figure 11a. When the concrete filling ratio was 0.2, the buckling position changed as the axial force ratio increased. On the other hand, when the concrete filling ratio was 0.4 or 0.6, buckling occurred at the base of the steel tube. With $L_c/L = 0.2$, the estimation equation gives a good approximation of the maximum bearing capacity in the numerical analysis. On the other hand, there was a difference between the numerical and estimated values for the model with $L_c/L = 0.4$ at low axial force ratios and for the model with $L_c/L = 0.6$ in general. These results were similar in Figure 11b–f, where the slenderness ratio varied, and the difference between the numerical and estimated values tended to increase as the concrete filling ratio increased.

4.2.2. Results for Varying Concrete Filling Ratios

Figure 12 plots the horizontal load bearing capacity for each concrete filling ratio and the value obtained by the estimation formula. The vertical axis shows the estimated value of P/P_u and the horizontal axis shows the numerical value of P/P_u. The open and closed dots in the figure show the numerical results.

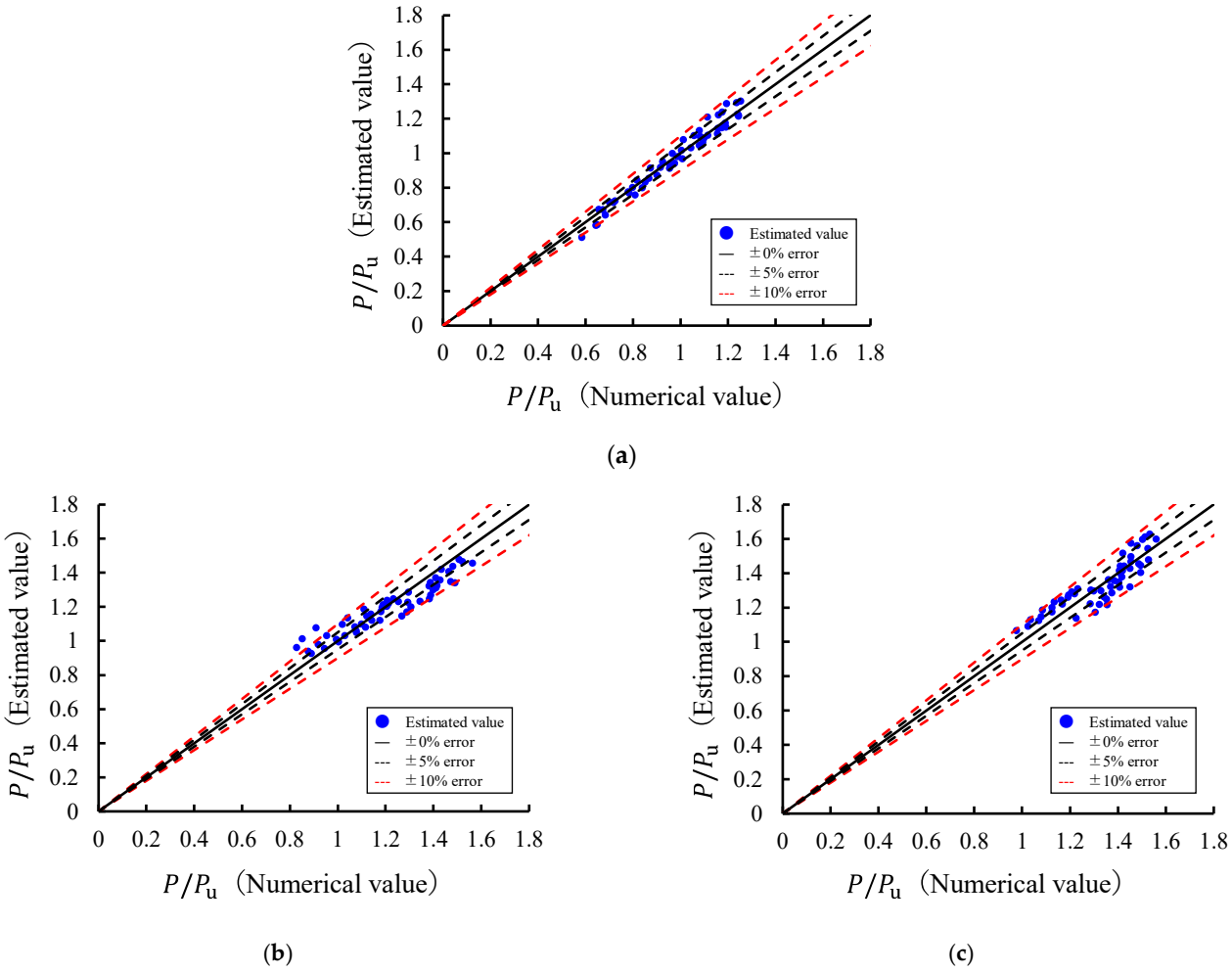

Figure 12. Difference between maximum load bearing capacity from numerical analysis and estimation equation: (**a**) $L_c/L = 0.2$; (**b**) $L_c/L = 0.4$; (**c**) $L_c/L = 0.6$.

In the model with $L_c/L = 0.2$, the difference between the numerical value and the estimated equation is generally within 5% in all cases, and the horizontal load bearing capacity of the model can be obtained by the estimated equation. For $L_c/L = 0.6$, the errors of most of the models ranged between 5% and 10%. From Sections 3 and 4.2, we believe these errors were generally between 5% and 10% because the estimated equations could not capture the increasing trend of the difference in horizontal load bearing capacity due to the differences in buckling position. In other words, although the least-squares method could be used to express the horizontal bearing capacity in a single equation, it was not possible to take into account the different tendencies of the horizontal bearing capacity arising from differing buckling positions.

5. Estimation Equation for Maximum Load Bearing Capacity Considering Buckling Position

Using the results of the previous sections, the location of buckling in PCFST is predicted by their design parameters. We studied the conditions for buckling at the base of the steel tube, buckling in two locations (at the base of the steel tube and just above the

concrete), as well as for buckling just above the concrete alone, and we propose an equation for the maximum load bearing capacity for each case.

5.1. Prediction of Buckling Position

A formula for estimating the position where buckling deformation will occur in PCFST is proposed, using the radius thickness ratio R, slenderness ratio λ, concrete filling ratio L_c/L , and axial force ratio n as parameters. The formula was obtained by linear discriminant analysis using the free statistical analysis software R, release 3.6.2, similar to the process of deriving the equation for estimating horizontal load bearing capacity. The formula for estimating buckling position using the various parameters and obtained by linear discriminant analysis is as follows:

$$f = 25 \times R + 0.40 \times \lambda + 3.97 \times n - 8.88 \times \frac{L_c}{L} + 0.04 \tag{5}$$

Here, it is predicted that buckling occurs only at the section just above the concrete if f is positive and that buckling occurs at the base, or at two locations, at the base and immediately above the concrete, if f is negative. Thus, the relationship is as follows:

$$f \begin{cases} > 0 & \ldots \text{buckling only at section just above concrete} \\ < 0 & \ldots \text{at base, or at base and just above concrete} \end{cases} \tag{6}$$

As representative examples, Figure 13 shows the relationship of the buckling position in the steel tube and the estimation formula for models C-009-020 and C-009-040. In the figure, open dots indicate cases where buckling occurred only at the section directly above the concrete and closed dots indicate cases where buckling occurred at the base, or at two locations as described above. The dashed line shows values from the formula for estimating buckling position. The figure shows that the buckling position is adequately classified. If the point is above the dashed line, buckling is predicted to occur at the base, or in the two locations noted earlier. Alternatively, if the point is below the line, buckling is predicted to occur only at the section directly above the concrete. The same tendency was also observed under other conditions, showing that the position where buckling of the steel tube occurs can be classified using this estimation formula.

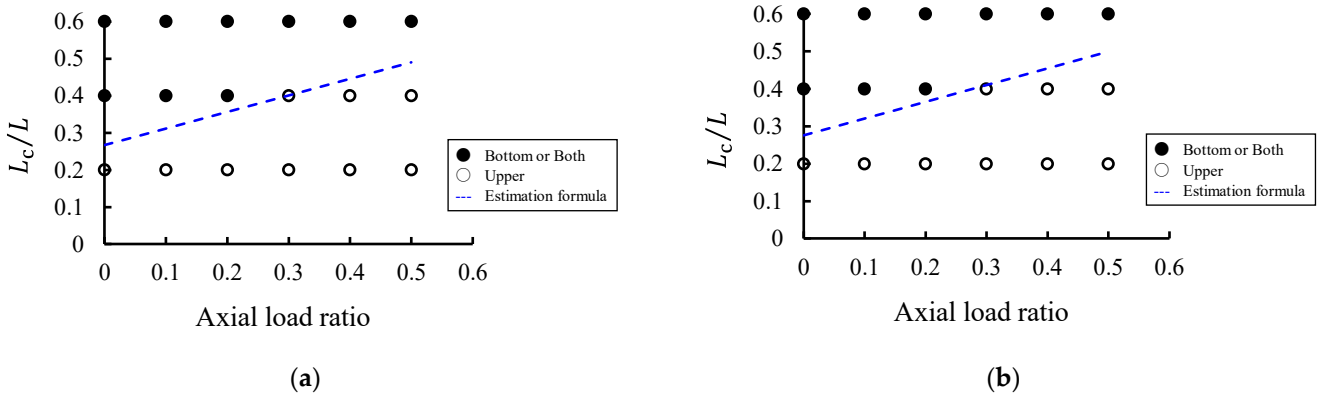

Figure 13. Buckling position relationships with n and L_c/L: (**a**) Model C-009-020; (**b**) Model C-009-040.

5.2. Proposed Estimation Equation

Nonlinear regression analysis was performed using the statistical analysis software R release 3.6.2 for each group of buckling positions in the PCFST discussed above. The estimation equation for the group where the steel tube buckled at the base, or in two locations, is shown in Equation (7). For the group where the steel tube buckled at the section just above the concrete, the estimation equation is shown in Equation (8).

$$\frac{P}{P_u} = \left(2.91 \times \frac{L_c}{L}^{0.06} \times R^{0.27} \times \lambda^{0.01}\right) - \left(0.15 \times \frac{L_c}{L}^{-0.31} \times R^{-0.72} \times \lambda^{0.84} \times n^{0.95}\right) \quad (7)$$

$$\frac{P}{P_u} = \left(2.02 \times \frac{L_c}{L}^{0.41} \times R^{-0.06} \times \lambda^{-0.03}\right) - \left(3.61 \times \frac{L_c}{L}^{0.37} \times R^{0.05} \times \lambda^{0.15} \times n^{1.34}\right) \quad (8)$$

P_u indicates the maximum bearing capacity at $L_c/L = 0$ and $n = 0$ for each model.

5.3. Applicability of Estimation Equations

In this section, the applicability of the estimation equations for maximum load bearing capacity taking the position where buckling occurs into account is evaluated by comparing their predictions with numerical analyses and experimental results.

5.3.1. Comparison with Numerical Analyses

As representative examples, Figure 14 shows the results of the numerical analysis and the values obtained from the estimation equations accounting for buckling locations for models C-009-020 and C-009-040. The vertical axis, horizontal axis, and legend are the same as in Figure 11. It can be seen that using the two estimation equations that consider buckling position yields better estimates of the maximum load bearing capacity than shown in Figure 11c,d, which use one estimation equation for the same conditions.

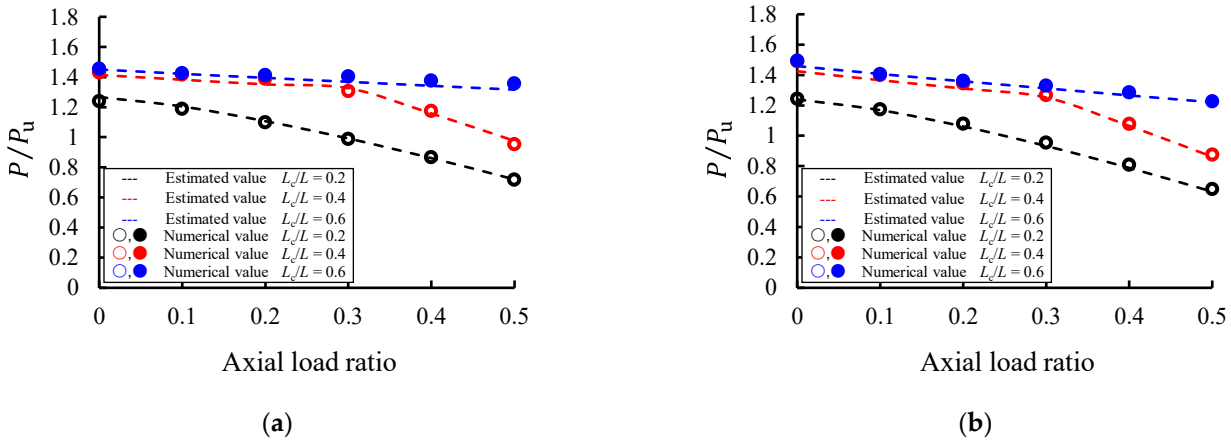

Figure 14. Maximum load bearing capacity and modified estimation equations for models C-009-020 and C-009-040: (**a**) Model C-009-020; (**b**) Model C-009-040.

Figure 15 plots the results from the numerical analysis and the estimation equations for all cases. The vertical axis shows the estimated value of P/P_u, while the horizontal axis shows the numerical value of P/P_u. The solid line in the figure indicates an error of 0%. The dashed lines indicate a range of error within ±5%, and the red dashed lines indicate a range of error within ±10%. Figure 15 shows that the difference between the numerical and estimated values was about 5% in all cases. Moreover, it can be seen that the errors that exceeded 10% in Figure 12, based on one estimation equation, have improved. Therefore, the maximum load bearing capacity can be accurately estimated within the scope of this study by using two estimation equations that account for the position where buckling occurred.

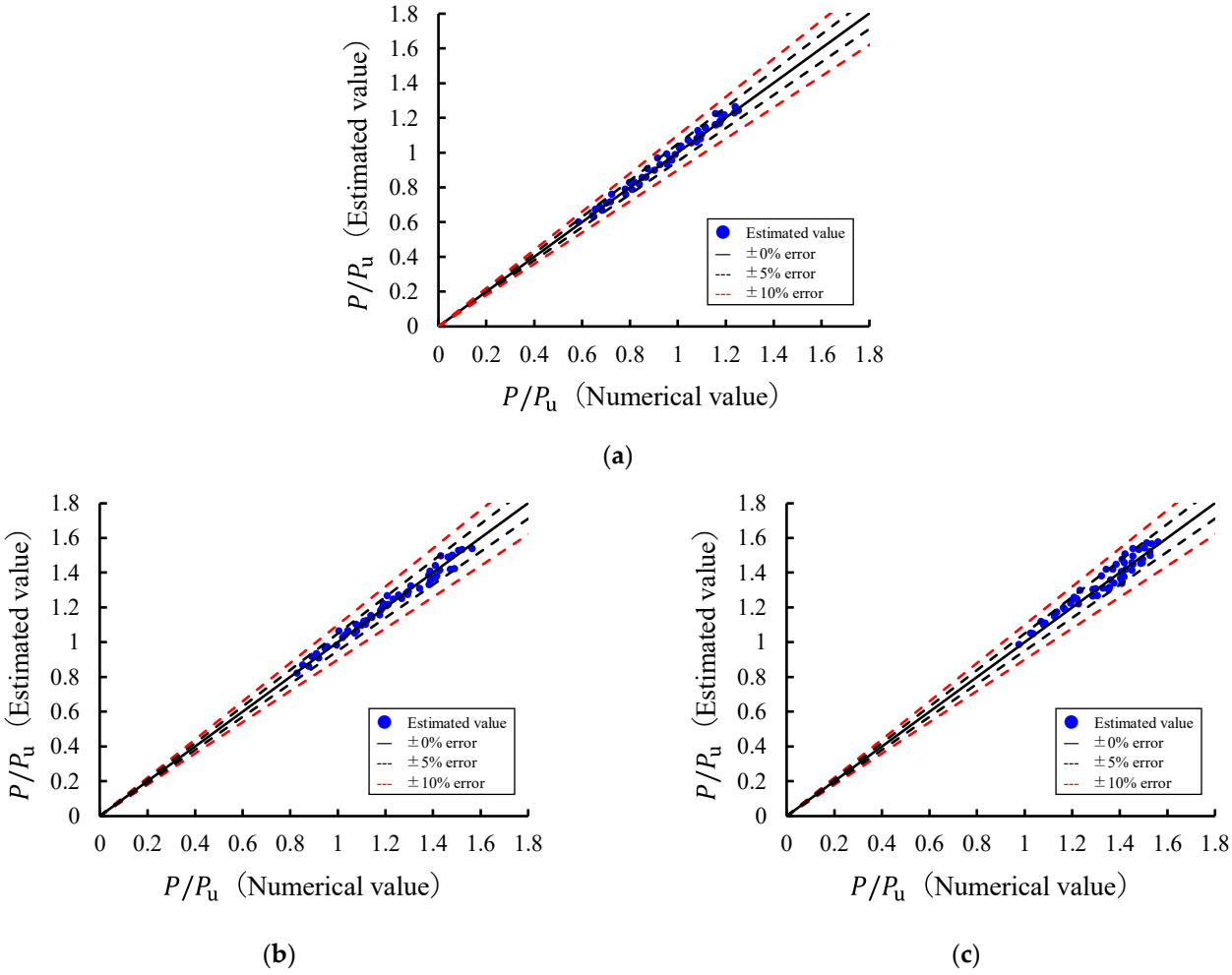

Figure 15. Difference between maximum load bearing capacity from numerical analysis and modified estimation equations: (**a**) L_c/L =0.2; (**b**) $L_c/L = 0.4$; (**c**) $L_c/L = 0.6$.

5.3.2. Comparison with Static Loading Experiments

The estimation equations were tried to apply to the horizontal load bearing capacity obtained in static loading experiments on concrete-filled steel tubes. Four models from experimental samples of concrete-filled steel tubes with circular cross-sections was used, based on studies by Iura et al. [8] and Morishita et al. [4] in the comparison. These samples were in the range of design parameters of Table 1, $0.03 \leq R \leq 0.12$, $0.2 \leq \lambda \leq 0.4$, $0.1 \leq n \leq 0.5$, and $0.2 \leq L_c/L \leq 0.6$.

Table 3 shows the various properties of each model. Note that these experiments were performed using cyclic loading, rather than monotonic lateral loading. According to Chapter 20 of the Guidelines for Stability Design of Steel Structures [16], the difference between monotonic and cyclic loading is not significantly large until maximum lateral loading is reached, but the number of cycles after peaking has been shown to have a large effect on the behavior of the members. Hence, the equations proposed in this study are deemed to also be applicable for estimating the maximum load bearing capacity under cyclic loading. To obtain the normalized horizontal load bearing capacity P/P_u, the horizontal load bearing capacity of the steel tube at $L_c/L = 0$ and $n = 0$ must be calculated. Since this property was tested in this study, P_u was obtained using the following equations [16,17].

$$\frac{P_u}{P_y} = \frac{0.02}{(R\lambda)^{0.8}} + 1.10 \tag{9}$$

$$P_y = \left(\frac{M_y}{h}\right)\left(1 - \frac{N}{N_y}\right) \tag{10}$$

Table 3. Experimental model specifications for comparison.

Reference	Iura et al. [9]		Morishita et al. [6]	
Model	C-008-030	C-009-032	C-1.5D-S	C-2D-S
Diameter of steel tube D [mm]	400		318.5	
Thickness of steel tube t_s [mm]	5.73	5.77	6.90	
Height of steel tube L [mm]	1750		1800	
Radius thickness ratio parameter R	0.08	0.09	0.058	
Slenderness ratio parameter λ	0.30	0.32	0.407	
Concrete filling ratio L_c/L	0.34		0.27	0.35
Axial force ratio n	0.15		0.20	
Buckling position	Bottom part		Bottom part	

Here, Equation (9) shows the horizontal yield strength P_y calculated taking the effect of axial force into account. The applicable range of Equation (9) is $0.03 \leq R \leq 0.11$ and $0.25 \leq \lambda \leq 0.5$.

In Iura et al. [8], static cyclic loading tests were conducted for varying diaphragm locations, concrete filling ratios, and loading methods in order to show their effects on horizontal bearing capacity and buckling position. Among the tested specimens are two models with diaphragms directly above the concrete, C-008-030 and C-009-032, which fit within the range of application of Equation (9), the horizontal load bearing capacity estimation equation for steel tubular columns with circular cross-sections. Model C-008-030 was subjected to three cyclic loadings and had a concrete filling ratio L_c/L of 0.34. Buckling occurred at the base of the steel tube. Model C-009-032 was subjected to one cyclic loading and had a concrete filling ratio L_c/L of 0.34. Buckling occurred at the base of the steel tube in that case as well. In Morishita et al. [4], quasi-static cyclic loading tests were conducted on concrete-filled circular steel tubular columns to show the effects of concrete filling ratio and the presence of a diaphragm installed directly above the concrete on the bearing capacity and deformation performance of the steel tubes. Among the tested specimens are two models with diaphragms, C-1.5D-S and C-2D-S, which satisfy the range of application of Equation (9), the horizontal load bearing capacity estimation equation for steel tubular columns with circular cross-sections. The concrete filling ratio L_c/L was 0.27 for C-1.5D-S and 0.35 for C-2D-S. Both models were subjected to three cyclic loadings and buckling occurred at the base of the steel tube.

Figure 16 summarizes the estimated and experimental values. Figure 16a plots the results when buckling position is not considered, while Figure 16b plots the results when buckling position is taken into consideration. The vertical axis shows the estimated values of P/P_u, while the horizontal axis shows the experimental values of P/P_u. The legend is the same as in Figure 12. Taking the buckling position into account, the estimate was smaller than the experimental value by 2% for C-008-030, but larger by 6% for C-009-032, by 3% for C-1.5DS, and by 6% for C-2D-S. The errors were within 10% for all cases regardless of the loading method, showing that the equations can provide estimates with high accuracy. On the other hand, if the buckling position is not taken into account, the estimation may result in errors as large as 10% as in C-008-030. This shows that the accuracy of the estimation equations improved, and the maximum load bearing capacity can be estimated with an error of about 5% when buckling position is taken into account. It was also found that without performing numerical analysis, the estimation formula shown in Equation (9) can be used to obtain the required P_u to estimate maximum load bearing capacity and can give maximum load bearing capacity estimates without producing large errors.

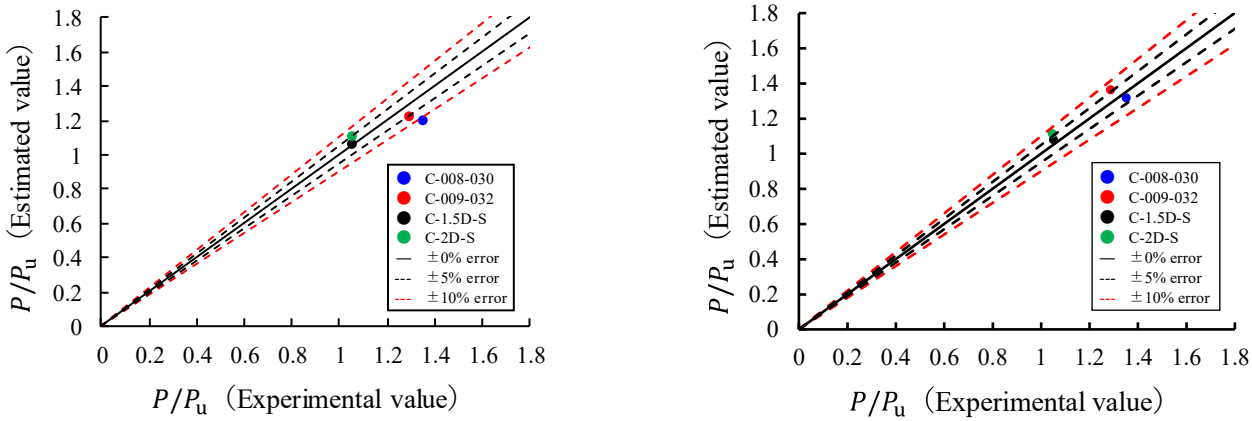

Figure 16. Comparison of experimental to estimated values: (**a**) Buckling position not considered; (**b**) Buckling position considered.

6. Conclusions

This study focused on four parameters (radius thickness ratio R, slenderness ratio λ, axial force ratio n, and concrete filling ratio L_c/L) used in numerical analysis to determine horizontal load bearing capacity and buckling position in concrete-filled circular section tubes with diaphragms under monotonic loading. Based on the results, an equation for estimating the horizontal load bearing capacity of concrete-filled tubes was obtained by nonlinear regression analysis and its applicability was evaluated. The results of this study are described below.

(1) Three buckling modes were identified: buckling at the base of the steel tube, buckling just above the concrete, and buckling in both locations. The mode depends on the radius thickness ratio R, the slenderness ratio λ, axial force ratio n, and concrete filling ratio L_c/L. When buckling at the base of the steel tube or buckling in both locations occurred, the horizontal load bearing capacity did not decrease significantly with the increase in the axial force ratio n, but with buckling just above the concrete, the horizontal load bearing capacity decreased rapidly.

(2) Although the slenderness ratio λ did not affect the buckling position of the steel tube, buckling just above the concrete was more likely to occur as both the radius thickness ratio R and the axial force ratio n increased in tubes with small concrete filling ratios L_c/L.

(3) The estimation equation that did not consider different buckling positions predicted the horizontal load bearing capacity with an error of approximately ±10% from the numerically analyzed values, but the error between the estimated and numerical values increases as the concrete filling ratio L_c/L increased from 0.4 to 0.6. On the other hand, the estimating equation that took the different buckling positions into consideration could predict the horizontal bearing capacity to within a margin of error of about 5% from the numerical value by determining the buckling position in advance.

(4) The accuracy of the estimating equation was verified based on previous experimental studies. The accuracy of the estimating equation was found to be within a margin of error of approximately ±10% from the experimental value when the buckling position was not taken into account, and approximately ±5% when the buckling position was taken into account.

In future work, it will be necessary to analyze models with different conditions such as diaphragms, stiffeners, and loadings in circular and rectangular cross-sections to clarify the effects of horizontal load bearing capacity and buckling position. Based on these results, a more comprehensive equation for estimating buckling position and horizontal bearing capacity will be studied.

Author Contributions: Conceptualization, Y.C.; methodology, Y.C.; software, S.Z.; validation, S.Z.; formal analysis, S.Z.; data curation, S.Z.; writing—original draft preparation, Y.C., S.Z. and S.S.; writing—review and editing, Y.C., S.Z. and S.S.; project administration, Y.C. All authors have read and agreed to the published version of the manuscript.

Funding: This research received no external funding.

Institutional Review Board Statement: Not applicable.

Informed Consent Statement: Not applicable.

Conflicts of Interest: The authors declare no conflict of interest. The funders had no role in the design of the study; in the collection, analyses, or interpretation of data; in the writing of the manuscript, or in the decision to publish the results.

References

1. Subcommittee on Investigation of Seismic Damage of Steel Structure. Investigation of Causes of Damage to Steel Structure on Hanshin-Awaji Earthquake Disaster. *J. JSCE* **2000**, *647*, 17–30. (In Japanese)
2. Han, L.H.; Yao, G.H.; Tao, Z. Behaviors of concrete-filled steel tubular members subjected to combined loading. *Thin Walled Struct.* **2007**, *45*, 600–619. [CrossRef]
3. Han, L.H.; Tao, Z.; Yao, G.H. Behavior of concrete-filled steel tubular members subjected to shear and constant axial compression. *Thin Walled Struct.* **2008**, *46*, 765–780. [CrossRef]
4. Morishita, M.; Aoki, T.; Suzuki, M. Experimental Study on the Seismic Resistance Performance of Concrete-Filled Steel Tubular Columns. *J. Struct. Eng.* **2000**, *46A*, 73–83. (In Japanese)
5. Zenzai, S.; Shimizu, S.; Chikahiro, Y.; Ohkami, T. Effect of Diaphragm on Seismic Behaviour of Partially Concrete-Filled Steel Tube. *Steel Constr. Eng.* **2019**, *26*, 25–36. (In Japanese) [CrossRef]
6. Hu, H.T.; Huang, C.S.; Chen, Z.L. Finite element analysis of CFT columns subjected to an axial compressive force and bending moment in combination. *J. Constr. Steel Res.* **2005**, *61*, 1692–1712. [CrossRef]
7. Goto, Y.; Kumar, G.P.; Kawanishi, N. Nonlinear finite-element analysis for hysteretic behavior of thin-walled circular steel columns with in-filled concrete. *J. Struct. Eng.* **2010**, *136*, 1413–1422. [CrossRef]
8. Iura, M.; Orino, A.; Ishizawa, T. Elasto-Plastic Behaviour of Concrete-Filled Steel Tubular Columns. *J. JSCE* **2002**, *696*, 285–298. (In Japanese) [CrossRef]
9. Japan Road Association. *Specification for Highway Bridges Part V: Seismic Design*; Japan Road Association: Tokyo, Japan, 2012; pp. 251–274.
10. Public Works Research Institute, Ministry of Construction. *Cooperative Research on a Limit State Design of Piers of Highway Bridge Under Seismic Loading (Summarized Edition)*; Public Works Research Institute, Ministry of Construction: Tsukuba, Japan, 1999; p. 51. (In Japanese)
11. American Concrete Institute. *Building Code Requirement for Structural Concrete and Commentary (ACI318-99)*; American Concrete Institute: Farmington Hills, MI, USA, 1999; p. 83.
12. Popovics, S. A Numerical Approach to the Complete Stress-Strain Curve of Concrete. *Cem. Concr. Res.* **1973**, *3*, 583–599. [CrossRef]
13. Chen, W.F. *Plasticity in Reinforced Concrete*; J. Ross Publishing: Fort Lauderdale, FL, USA, 2007; pp. 19–48.
14. Johansson, M.; Gylltoft, K. Structural behavior of slender circular steel-concrete composite columns under various means of load application. *Steel Compos. Struct.* **2001**, *1*, 393–410. [CrossRef]
15. Ngo, D.; Scordelis, A.C. Finite Element Analysis of Reinforced Concrete Beams. *J. Proc.* **1967**, *64*, 152–163.
16. JSCE/Committee on Steel Structure. *Guidelines for Stability Design of Steel Structures*, 2nd ed.; Japan Society of Civil Engineers: Tokyo, Japan, 2005; pp. 428–429. (In Japanese)
17. Usami, T.; Ge, H.B. Cyclic behavior of thin-walled steel structures-numerical analysis. *Thin Walled Struct.* **1998**, *32*, 41–80. [CrossRef]